Intermediate-range order in aqueous solutions of salts: a systematic computer simulation study

2005 J. Phys.: Condens. Matter 17 453

(http://iopscience.iop.org/0953-8984/17/3/004)

INSTITUTE OF PHYSICS PUBLISHING JOURNAL OF PHYSICS: CONDENSED MATTER

J. Phys.: Condens. Matter **17** (2005) 453–467 doi:10.1088/0953-8984/17/3/004

Intermediate-range order in aqueous solutions of salts: a systematic computer simulation study

Mauro C C Ribeiro

Laboratório de Espectroscopia Molecular, Instituto de Química, Universidade de São Paulo, CP 26077, CEP 05513-970, São Paulo, SP, Brazil

E-mail: mccribei@quim.iq.usp.br

Received 27 October 2004, in final form 13 December 2004
Published 7 January 2005
Online at stacks.iop.org/JPhysCM/17/453

Abstract

Molecular dynamics (MD) simulations of aqueous ionic solutions have been performed in order to identify intermediate-range order (IRO), that is, spatial correlation between species beyond nearest-neighbour distances. The effect of increasing concentration and cation charge (M^+, M^{2+}, and M^{3+}) on IRO is systematically investigated. Spatial correlation between cations at relatively long range is probed in both real space at about 10.0 Å by radial distribution functions, and in reciprocal space at about 0.8 $Å^{-1}$ by static structure factors. Well defined correlation between cations with elevated charge at this distance has been observed, that is in full agreement with the quasi-close-packing model proposed on the basis of x-ray diffraction measurements on ionic solutions. Time correlation functions of density fluctuation at different wavevectors have been calculated. These correlation functions indicate that the timescale of structural relaxation in the spatial range typical of IRO is very slow in the case of concentrated solutions containing M^{2+} or M^{3+} cations.

1. Introduction

Computer simulation is now an established technique for revealing the microscopic structure and dynamics of aqueous ionic solutions. The technique is particularly suitable for systematic investigations of, for instance, ionic size effects on the equilibrium structure and dynamics of solutions. The most investigated systems are certainly aqueous solutions of alkaline halides [1–10], although polyatomic ions such as NO_3^- [11], ClO_4^- [12], NH_4^+ [13], etc, have also been studied. Usually, infinitely diluted solutions have been simulated in which a single ion is considered [1–3], but concentration effects have also been addressed [4–10]. Recurrent issues in these studies are the structure and residence time of water molecules in the first-hydration shell around the ions, and, in the case of concentrated solutions, the formation of ionic pairs in direct contact.

The mentioned computer simulations are thus concerned with short-range order given by nearest neighbour species in ionic solutions. On the other hand, in a continued x-ray diffraction investigation by Marques, Cabaço and co-workers [14–21], it has been found that an intermediate-range order (IRO) develops in aqueous solutions containing di- or trivalent cations. The IRO is manifest in the static structure factor, $S(k)$, by the occurrence of a *pre-peak*, which is a peak at relatively low wavevector, $k \sim 0.9$ Å^{-1}. This k range is below the main peak of $S(k)$, so that the pre-peak indicates the presence of order in a relatively extended spatial range, say 10.0 Å in real space. The phenomenology of IRO in aqueous solution can be summarized as follows. IRO develops when high-valence ions are present (Ca^{2+}, Mg^{2+}, Cu^{2+}, Al^{3+}, Y^{3+}, and many others), and it has also been observed with aqueous solution of divalent anions, for instance $LiSO_4$ [19]. By increasing the concentration, the magnitude of the pre-peak increases and its position shifts to higher k. The intensity of the pre-peak increases with increasing scattering power of the largest valence ion, but decreases if the scattering power of the counter-ion increases when it is not close to the high valence ion.

It is well known that many glass-forming liquids display a pre-peak in $S(k)$, but the actual nature of the corresponding IRO is an issue of lively debate because different explanations have been proposed [22–24]. Neutron scattering spectroscopy and computer simulations of molten salts and organic liquids have been intensively used to characterize the structural pattern that is responsible for the IRO. In the case of the archetypical glass-forming liquid SiO_2, IRO is due to correlations in the network of connected SiO_4^{2-} tetrahedra [25]. However, it has also been suggested that IRO may arise from correlation of voids or layers in the bulk of a supercooled liquid [26]. It has been shown that IRO in *m*-toluidine is due to clusters in a network of hydrogen-bonded molecules [27]. In a group of molten salts, the pre-peak in $S(k)$ was observed by computer simulations as long as polarizable models were employed [28]. In the case of aqueous solutions of salts, x-ray diffraction data have been satisfactorily reproduced with a simple structural model [14–21]. In this model, a hypothetical cubic arrangement is assumed for the high valence cations, this structural pattern being called a liquid-type quasi-close-packing. Taking into account the available volume, cations are positioned with a relatively long distance between each other, about 10.0 Å, in order to minimize strong Columbic repulsions between M^{2+} or M^{3+} species. The first shells around the cations include water molecules and anions, these being the scattering units responsible for the observed pre-peak in $S(k)$. Free anions and water molecules are distributed in available holes of this large cubic lattice. Anions at mid-points between two cations contribute destructively to the intensity of the pre-peak. Beyond a reasonable distance from a given central particle, a uniform random distribution is assumed. With such a simple model, good agreement between calculated and experimental $S(k)$ was achieved for many different ionic solutions [14–21].

The purpose of this work is to reveal the nature of IRO in ionic solutions by using molecular dynamics (MD) simulations. In contrast to previous MD simulations of ionic solutions, which were mainly concerned with the (short-range) structure of hydration shell, the main issue in this work is the spatial order at relatively long distances. Instead of focusing on a particular system, simple models have been used, allowing a systematic view of the trends of IRO in aqueous solutions when basic features are changed, namely, the ionic charge and concentration. However, the starting model is a realistic one, in the sense that it mimics LiCl aqueous solutions. From this starting model, we systematically changed it by assigning +2 or +3 formal charge to the cations. We address the effect of ion size by changing the parameters of the short-range part of the potential energy function. The effect of increasing temperature on the structure of the simulated systems was also investigated. Equilibrium structures of the simulated systems are investigated in both the real space, by using radial distribution functions, $g(r)$, and in the reciprocal space by $S(k)$. Overall, the MD simulations corroborate

Table 1. The systems simulated in this work: the number of water molecules and ions, and the size of the cubic box used in the MD simulations at 300 K.

Solutions		H_2O	Anions	Cations	Box (Å)
I	MX	960	20	20	30.97
	MX_2	970	20	10	30.86
	MX_3	960	30	10	30.71
II	MX	880	60	60	30.77
	MX_2	880	80	40	30.58
	MX_3	880	90	30	30.68
III	MX	800	100	100	30.56
	MX_2	820	120	60	31.00
	MX_3	800	150	50	30.75

the quasi-close-packing model put forward to explain IRO in ionic solutions [14–21], but add a further detailed microscopic view as one expects from a computer simulation investigation. Furthermore, MD simulations give insight on the timescale of structural relaxation in this spatial range, that is, the corresponding IRO *dynamics* in aqueous ionic solutions.

2. Computational details

The MD simulations were performed with a potential energy function including short-range Lennard-Jones and long-range Coulombic interactions. The model for water is the well known SPC/E model [29]. The Lennard-Jones parameters, ε and σ, corresponding to Li^+ and Cl^- species, were taken from [30]. Keeping the Lennard-Jones parameters fixed and replacing the full +1 formal charge of cations to +2 or +3, we generated models for aqueous solution of MCl, MCl_2, and MCl_3 salts. Cross-term parameters for interactions between different species are given by usual combining rules: $\varepsilon_{ij} = (\varepsilon_{ii}\varepsilon_{jj})^{1/2}$ and $\sigma_{ij} = \frac{1}{2}(\sigma_{ii} + \sigma_{jj})$. Polarization effects were not considered in the models.

The MD simulations were performed in a cubic cell containing 1000 species. For each of the three cations (M^+, M^{2+}, and M^{3+}), three different concentrations were simulated by replacing an appropriate number of water molecules by ions. Thus, nine different solutions were simulated, and table 1 collects the number of water molecules, anions and cations considered. Taking LiCl as the reference salt, the three concentrations for the MCl solutions correspond to about 1.0, 2.0, and 4.0 M. In each case, the total number of ions (cations plus anions) was approximately maintained in each concentration respecting the MCl, MCl_2, and MCl_3 stoichiometry. For brevity of notation, M^+, M^{2+}, and M^{3+} systems at different concentrations will be called solution I, solution II, and solution III. The mass of both the M^{2+} and the M^{3+} species was kept the same as the lithium mass.

The dynamics of structural relaxation of concentrated M^{2+} and M^{3+} solutions is very slow. In fact, a concentrated aqueous solution of LiCl is a model glass-forming liquid system [31–34]. Due to such slow dynamics, several tests were performed to insure that the equilibrium structures discussed here are meaningful. All of the ionic solutions were generated from very different well equilibrated arbitrary configurations of pure water by random replacing of water molecules by ions. Typically after about 100.0 ps of equilibration run, in which the size of the cell is allowed to vary by using the Berendsen barostat [35] in order to result in an average pressure of 1.0 bar at 300 K, the equilibrium volume of each ionic solution is achieved. One obtains the same radial distribution functions as reported here if very different initial configurations are employed. As an alternative procedure, in the case of the MCl_3 solution III,

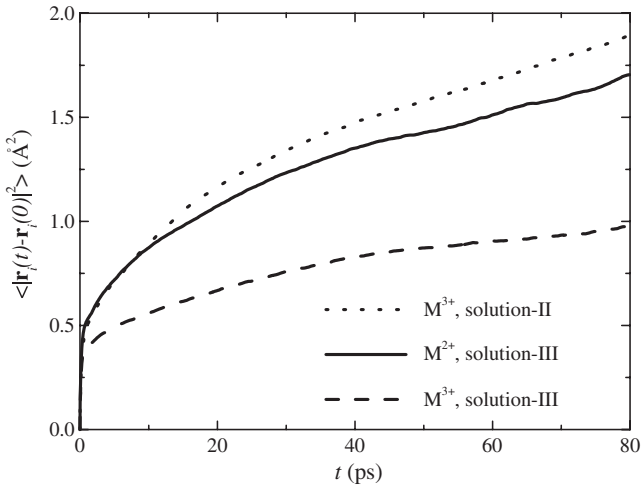

Figure 1. Average mean-square displacements of cations in MCl_2 solution III (full curve), MCl_3 solution II (dotted curve), and MCl_3 solution III (dashed curve).

we performed a sequential cooling (1000, 900, 800, ..., 300 K) with a 100.0 ps equilibration run at each temperature. Again, the same equilibrium structure was obtained (see figure 12). Another interesting way to verify that the cation correlations discussed here are reliable is to perform a swap of cation and anion positions of an arbitrary equilibrated configuration. After such a swap, we obtain a random distribution of cations, but the same structural pattern is then recovered by letting the system re-equilibrate for about 100.0 ps. Finally, in order to verify that a diffusive regime of ionic displacements was obtained during production runs, figure 1 shows the average mean-square displacement of cations (MSD), $\langle|\mathbf{r}_i(t) - \mathbf{r}_i(0)|^2\rangle$, where $\mathbf{r}_i(t)$ is the coordinate of ion i at time t, for some selected systems. Although the magnitude of calculated MSD indicates low ionic mobility in the simulated systems (see also section 3.6), figure 1 shows that a diffusive regime is achieved after about 50.0 ps.

Production runs were not less than 100.0 ps long, with a time-step of 1.0 fs, in which the size of the cubic box was fixed at the equilibrium value given in table 1. The size of the cubic box was typically $L \sim 31$ Å, so that the smallest wavevector available in the simulations was $k = 2\pi/L = 0.2$ Å^{-1}. Thus, the simulated systems are appropriate for investigating IRO in ionic solutions as pre-peaks in $S(k)$ are observed at $k \sim 0.9$ Å^{-1} [14–21]. During production runs, the Berendsen thermostat [35] was kept turned on with a small system–batch coupling parameter (0.1 ps). The water molecule was considered as a rigid body, and translational and rotational equations of motion were integrated with leap-frog algorithms [36]. Long-range Coulombic interactions were handled with the Ewald sum method [36], in which the damping parameter of the real space summation was $\alpha = 5.0/L$, and 50 vectors were considered in reciprocal space by using a wavevector cut-off of $k = 2.6$ Å^{-1}. In order to verify whether the long-range correlation between cations was dependent on how the reciprocal part of the Ewald sum was performed, a further test was done in the case of the MCl_2 solution II. This system was re-equilibrated by using a much larger number of wavevectors, actually 1799 vectors with a wavevector cut-off of $k = 12.1$ Å^{-1}. The same structural pattern was observed in both cases. As discussed in the following sections, further simulations were performed in order to check specific findings. For some of the systems shown in table 1, we changed the Lennard-Jones parameters so that the cation would mimic Na^+ or K^+ [30], and we doubled the charge of the anion in order to have a M_2X_2 salt.

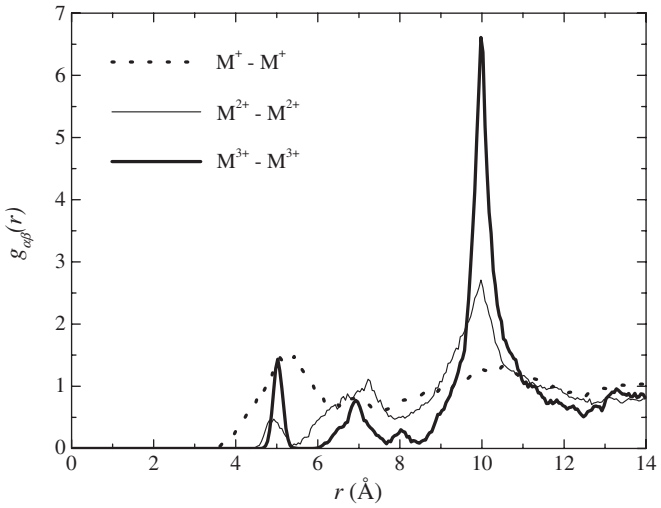

Figure 2. Partial cation–cation radial distribution functions, $g_{\alpha\beta}(r)$, calculated by MD simulations of M^+, M^{2+}, and M^{3+} solutions II.

3. Results

3.1. Charge effect

It has been proposed that the pre-peak in $S(k)$ of ionic solutions, and the associated IRO, arises from spatial correlation between high-valence cations [14–21]. Figure 2 shows calculated partial cation–cation radial distribution functions, $g_{\alpha\beta}(r)$, calculated by MD simulations of solutions II. The remarkable effect of increasing the cation charge is clear from figure 2: most noticeable, the increase in intensity of a sharp peak at about 10.0 Å. The main conclusion drawn from figure 2 is that MD simulations fully corroborate the most fundamental assumption of the quasi-close-packing model of [14–21], in which high-valence cations are placed with relatively long distances between each other in order to minimize Coulombic repulsions. Figure 2 gives further details on the actual structure of these solutions that are not present in the quasi-close-packing model, namely, the occurrence of cation–cation pairs at shorter distances, as given by peaks at about 5.0 and 7.0 Å. A natural question is then the structural motif of a cation pair at these short distances. Figure 3 shows the partial oxygen–cation and anion–cation $g_{\alpha\beta}(r)$ of MCl and MCl_3 solutions II. Nearest-neighbour species around cations include water molecules and anions located at about 2.0 and 2.5 Å, respectively. The first shell around cations is very well defined, as indicated by the sharp first peaks and deep first minima in $g_{\alpha\beta}(r)$ shown in figure 3. As expected, the first peak in these $g_{\alpha\beta}(r)$ shifts to smaller distances when the cation charge increases. Consistently, anion–cation $g_{\alpha\beta}(r)$ in the bottom panel of figure 3 present a valley at 10.0 Å, where the cation–cation $g_{\alpha\beta}(r)$ in figure 2 display a strong peak.

By selecting the nearest-neighbour species around cations, we constructed histograms of distribution of water molecules and anions that constitutes the first shell around cations. Histograms for solutions II are shown in figure 4. We found tetrahedral coordination in the case of MCl, and octahedral coordination in the case of MCl_2 and MCl_3 solutions. Most cations have their first solvation shell made of water molecules with eventual replacement of a single water molecule by an anion, but significant population of two or even three anions around a given cation could be discernable. Thus, the first shell is made of different numbers

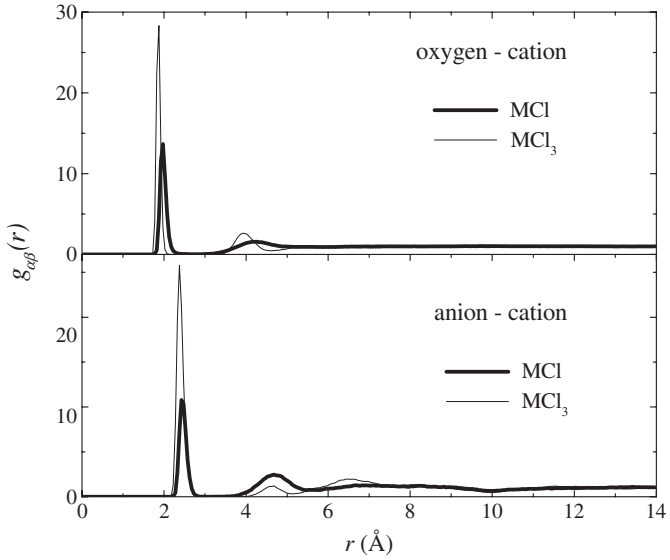

Figure 3. Partial oxygen–cation and anion–cation $g_{\alpha\beta}(r)$ calculated by MD simulations of MCl and MCl_3 solutions II.

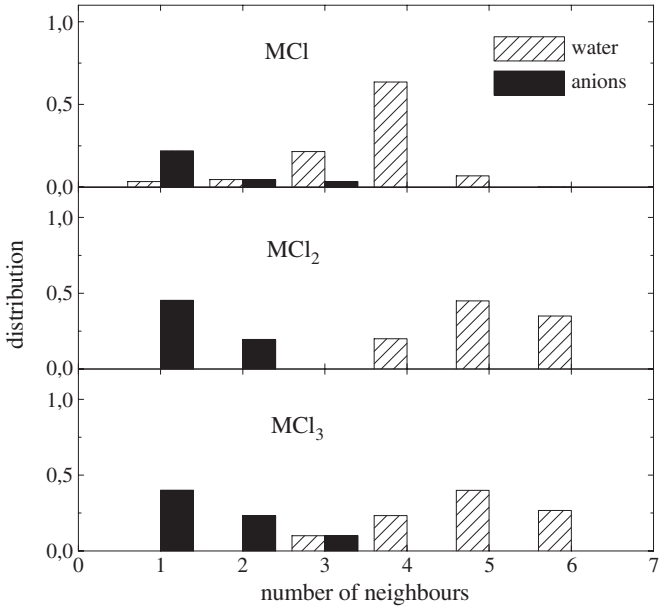

Figure 4. Histograms of nearest-neighbour anions and water molecules around a given cation in M^+, M^{2+}, and M^{3+} solutions II.

of water molecules and anions, giving a total of either four or six species around a given cation. By direct visualization of arbitrary configurations, one identifies that close approach of about 5.0 Å between high valence cations (see figure 2) is allowed by sharing an anion located at the vertex of an adjacent octahedron. Thus, the anion in between two cations screens the strong repulsion of the cations, and allows their close approach. The second peak at about 7.0 Å

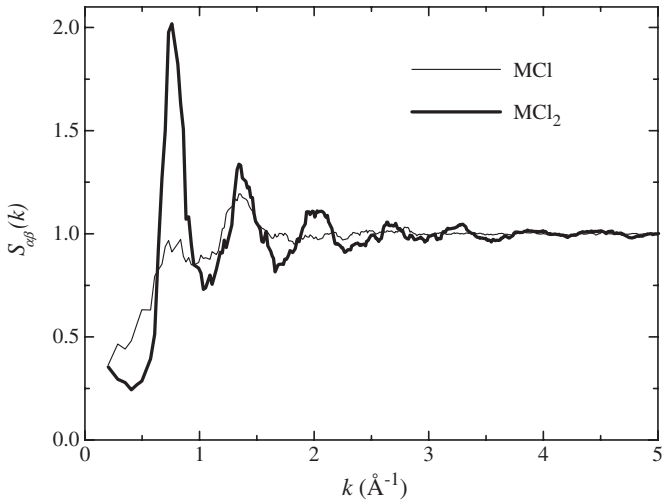

Figure 5. Partial cation–cation static structure factors, $S_{\alpha\beta}(k)$, calculated by MD simulations of MCl and MCl_2 solutions II.

in the partial cation–cation $g_{\alpha\beta}(r)$ (figure 2) arises from a less effective screening of cation interaction by water molecules in two complete adjacent octahedra.

IRO in these solutions arises from the intense peak at 10.0 Å in cations $g_{\alpha\beta}(r)$ shown in figure 2. It is not recommended to calculate partial $S_{\alpha\beta}(k)$ by Fourier transforming the corresponding $g_{\alpha\beta}(r)$. Instead, we calculated $S_{\alpha\beta}(k)$ directly by its definition [37]:

$$S_{\alpha\beta}(k) = \frac{1}{\sqrt{N_\alpha N_\beta}}\left\langle \sum_{i\in\alpha}^{N_\alpha}\sum_{j\in\beta}^{N_\beta} \mathrm{e}^{\mathrm{i}\mathbf{k}\cdot(\mathbf{r}_i-\mathbf{r}_j)}\right\rangle, \tag{1}$$

where $\mathbf{r}_i$ is the coordinate of species i, and α and β stands for each species. Figure 5 shows the cation–cation $S_{\alpha\beta}(k)$ for MCl and MCl_2 solutions II. The remarkable feature in figure 5 is well defined oscillations in $S_{\alpha\beta}(k)$ for M^{2+} cations in aqueous solution. The corresponding result for MCl_3 is not shown, as it is very similar to MCl_2. The intense peak at $k \sim 0.8$ Å^{-1} is responsible for the pre-peak observed in the experimental total $S(k)$, after proper weighing by concentration and length scattering of each species. Figure 6 shows partial $S_{\alpha\beta}(k)$ for the centre of mass of water molecules in MCl and MCl_2 solutions II. For comparison purposes, the corresponding $S_{\alpha\beta}(k)$ for pure water is also shown by a dashed curve. The most interesting characteristics is that low-k features also develop in partial water–water $S_{\alpha\beta}(k)$ in the case of ionic solutions. The occurrence of a pre-peak in water–water $S_{\alpha\beta}(k)$ is a direct consequence of water molecules in the hydration shell around the high-valence cations. This is corroborated in the inset of figure 6, which displays two water–water $S_{\alpha\beta}(k)$ which have been calculated assuming that a given water molecule belongs or does not belong to the hydration shell of any cation. The pre-peak in the water–water $S_{\alpha\beta}(k)$ is an obvious consequence of water molecules that follow the cation in its hydration shell. It should be noted that the k range of the main peak in figure 6 is also modified on going from pure water to ionic solutions. In pure water, the main peak at about 3.0 Å^{-1} is preceded by a shoulder at about 2.0 Å^{-1} (dashed curve in figure 6). In the case of ionic solutions, features in this range are broadened, and it seems that the relative magnitude of the peak at 2.0 Å^{-1} increases in comparison with the peak at 3.0 Å^{-1}. MD simulation of pure water has shown that the peak at 2.0 Å^{-1} is due to correlation of voids in the bulk of the liquid [38].

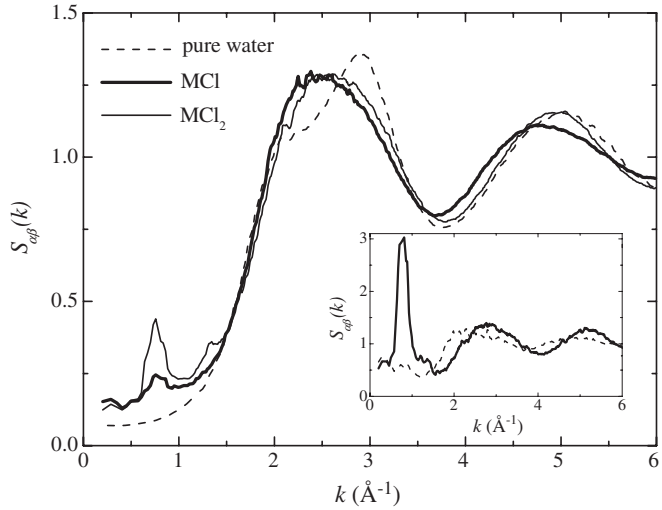

Figure 6. Partial water–water $S_{\alpha\beta}(k)$ calculated by MD simulations of MCl and MCl_2 solutions II. For comparison purposes, the corresponding result in pure water is shown by a dashed curve. The inset shows $S_{\alpha\beta}(k)$ of water molecules that belong (bold curve) or do not belong (dashed curve) to the hydration shell of any M^{2+} cation.

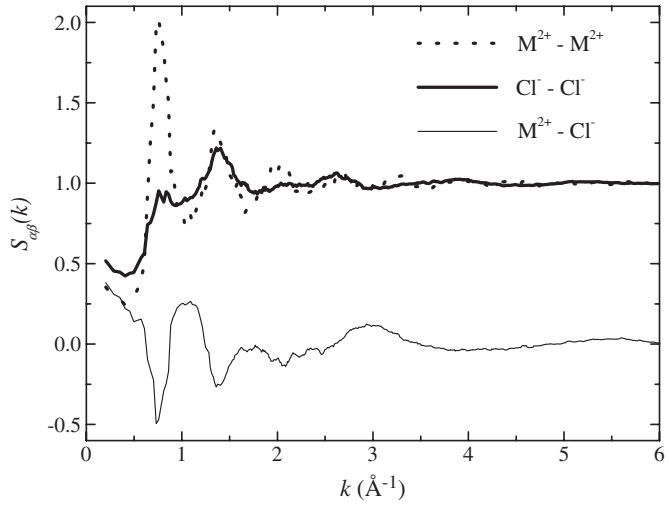

Figure 7. Partial cation–cation, anion–anion, and cation–anion $S_{\alpha\beta}(k)$ calculated by MD simulations of the MCl_2 solution II.

Finally, one argues that counter-ions that are not close to high-valence cations will contribute destructively to the intensity of the pre-peak when its scattering power increases [14–21]. Figure 7 shows the cation–cation, anion–anion, and cation–anion $S_{\alpha\beta}(k)$ for the MCl_2 solution II. Figure 7 indicates that the cation–anion interferes destructively with the cation–cation $S_{\alpha\beta}(k)$ at low k, so that the magnitude of the resulting pre-peak in the total $S(k)$ will decrease if one increases the weight given by the anion scattering power. Thus, MD simulations corroborate the most important assumptions of the quasi-close-packing model for IRO in ionic solutions [14–21].

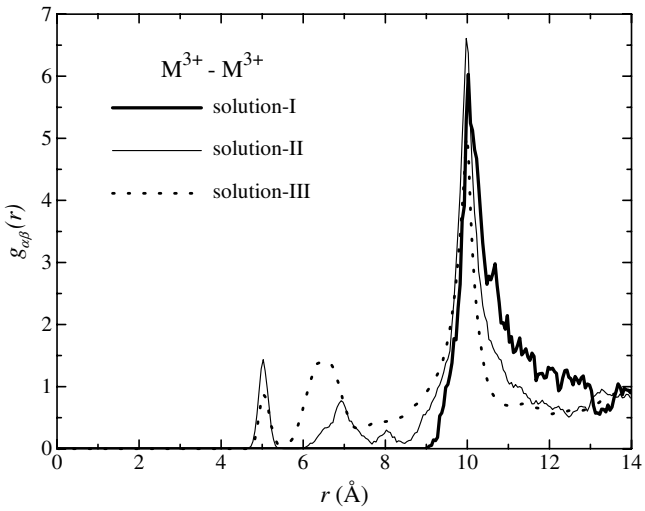

Figure 8. Partial M^{3+}–M^{3+} $g_{\alpha\beta}(r)$ calculated by MD simulations of solution I, solution II, and solution III.

3.2. Concentration effect

Figure 8 shows the M^{3+}–M^{3+} partial $g_{\alpha\beta}(r)$ calculated by MD simulations of three different concentrated solutions (see table 1). The peak at 10.0 Å is already present in solution I, and it sharpens with increasing concentration. As the peaks at about 5.0 and 7.0 Å arise by sharing of octahedra made of a cation plus its hydration shell, a low concentration of such octahedra implies that these peaks are absent from solution I. The important conclusion to be drawn from figure 8 is that the elevated charge of cations is the main reason for the long-range correlation in cation positions, and such order becomes more defined when concentration increases. Consequently, figure 9 shows that oscillations in cation–cation $S_{\alpha\beta}(k)$ becomes more pronounced (more solid-like $S_{\alpha\beta}(k)$) by increasing concentration. The slight shift of the peaks to higher k with increasing concentration in figure 9 should be noted. This is also observed in figure 10, which shows the partial water–water $S_{\alpha\beta}(k)$ of MCl_3 solutions. Thus, figures 9 and 10 indicate that the pre-peak in the total $S(k)$ of the ionic solution should increase and shift to higher k by increasing the concentration. In fact, it has been observed by x-ray diffraction measurements [14–21] that the pre-peak shifts as $c^{1/3}$, where c is the molar concentration. By considering the number density of cations of MCl_3 solutions (see table 1), and by measuring the corresponding first peak in the cation $S_{\alpha\beta}(k)$, the inset in figure 9 shows that such dependence is also obeyed in the simulated systems.

3.3. Cation size effect

Further MD simulations were performed by keeping cation charge and concentration fixed, and changing the Lennard-Jones parameters in order to simulate cations of different sizes. For instance, the Lennard-Jones parameters appropriate for Li^+ were replaced by the parameters for K^+ as given in [30]. As a representative example, figure 11 compares the partial M^{2+}–M^{2+} $g_{\alpha\beta}(r)$ for small and large cation sizes in the case of solution II. The peak at 10.0 Å is not affected by increasing the cation size because in such a spatial range the cations are so distant from each other that their relative position is barely affected by increasing their radius. On the

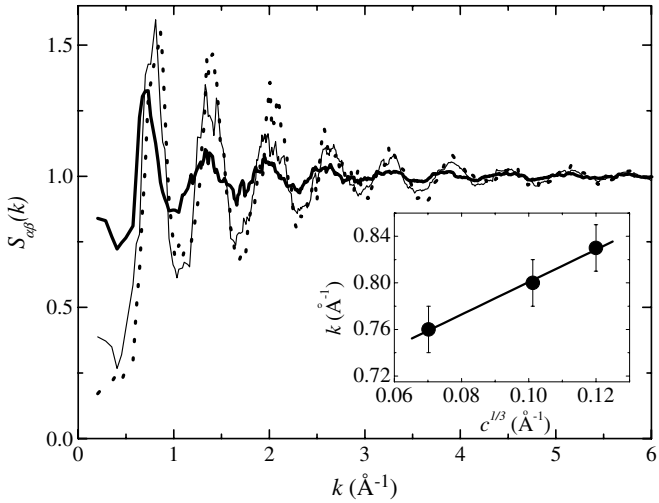

Figure 9. Partial M^{3+}–M^{3+} $S_{\alpha\beta}(k)$ calculated by MD simulations of solution I (bold curve), solution II (thin curve), and solution III (dashed curve). The inset shows the wavevector corresponding to the first peak of these $S_{\alpha\beta}(k)$ as a function of $c^{1/3}$, where c is the number density of cations in the simulated systems (see table 1). The error bars give the uncertainty in measuring the position of the first peak in $S_{\alpha\beta}(k)$.

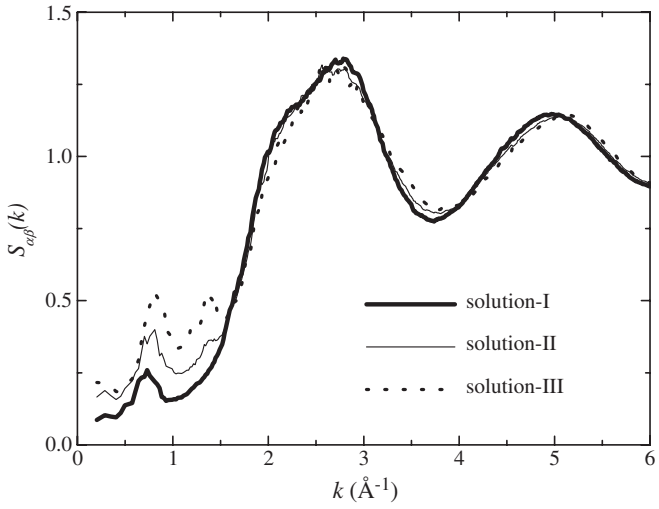

Figure 10. Partial water–water $S_{\alpha\beta}(k)$ calculated by MD simulations of MCl_3 solution I, solution II, and solution III.

other hand, the first peak at about 5.0 Å shifts to larger distance because it is due to a pair of cations that share a common anion, i.e. it is a short-range feature that responds to an increase in cation size. As the long-range correlation between cations was not affected by increasing cation size, the oscillatory pattern in the corresponding $S_{\alpha\beta}(k)$ is very similar to previous ones, and they are not shown here.

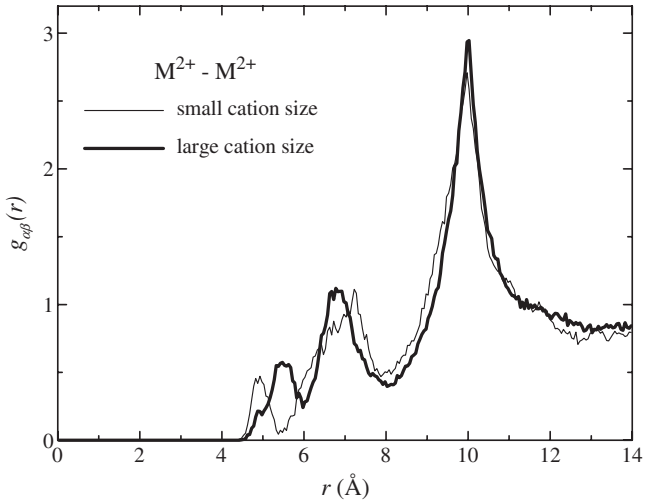

Figure 11. Partial M^{2+}–M^{2+} $g_{\alpha\beta}(r)$ calculated by MD simulations of MCl_2 solution II with different cation Lennard-Jones parameters.

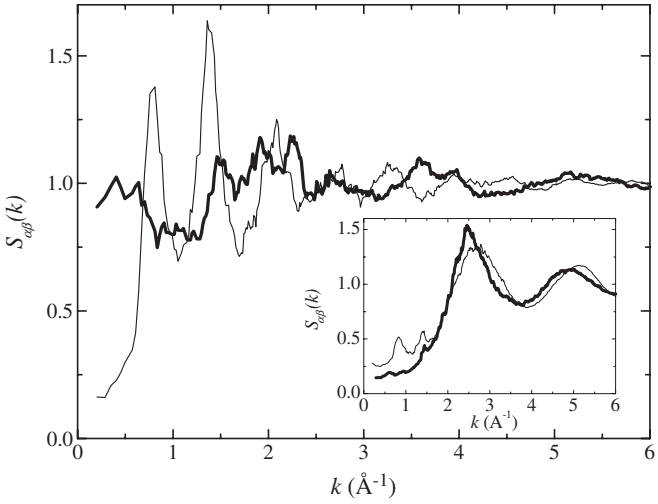

Figure 12. Partial M^{2+}–M^{2+} $S_{\alpha\beta}(k)$ calculated by MD simulations of MCl_2 (thin curve) and M_2Cl_2 (bold curve) solutions III. The inset shows the corresponding result for the water–water $S_{\alpha\beta}(k)$.

3.4. Anion charge effect

IRO in ionic solutions arises from an asymmetry in ionic charges, i.e. the presence of high-charge M^{2+} or M^{3+} cations and X^- anions. Thus, one expects that the pre-peak in $S_{\alpha\beta}(k)$ and the corresponding IRO would disappear in the case where both species have the same charge in modulus. This finding was corroborated by running MD simulations in which the anions had their charge doubled in solution III (actually, 820 H_2O, 90 M^{2+}, and 90 X^{2-}). Figure 12 shows the remarkable difference between the $S_{\alpha\beta}(k)$ of MCl_2 and M_2Cl_2. The pronounced oscillation in the cation–cation $S_{\alpha\beta}(k)$ in MCl_2 (thin curve) is washed out on going to M_2Cl_2 (bold curve). The inset shows that the pre-peak also disappears in the partial water–water $S_{\alpha\beta}(k)$ in the case of M_2Cl_2.

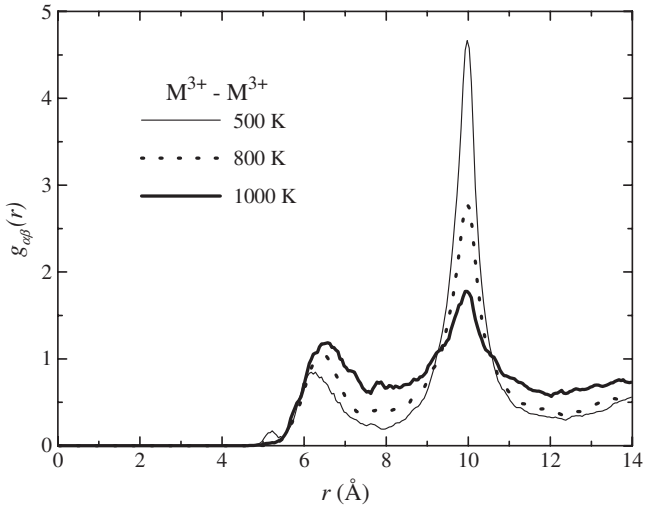

Figure 13. Partial M^{3+}–M^{3+} $g_{\alpha\beta}(r)$ calculated by MD simulations of MCl_3 solution II at 1000, 800, and 500 K.

3.5. Temperature effect

Finally, we test the effect of increasing temperature on long-range cation correlations. The results shown in figure 13 correspond to a sequential cooling of the MCl_3 solution III from 1000 K down to 300 K, that was used in an equilibration period of this system. In spite of unphysical temperature values, figure 13 shows the cation–cation $g_{\alpha\beta}(r)$ at 1000, 800, and 500 K in order to indicate that long-range cation correlation is already developed at high temperature, becoming pronounced and well defined with decreasing temperature. The peak at about 5.0 Å^{-1} shows a pronounced temperature effect, as it arises from short-range effects of octahedral sharing. Thus, figure 13 strongly suggests a physical picture that the quasi-close-packing model of cations continues to be valid at high temperature, due to strong Coulombic repulsion between cations, in spite of the increasing mobility of the molecules at higher temperature. Consequently, one expects that long-range spatial order in these ionic solutiona should have relatively long lifetime, as is in fact corroborated in the next section.

3.6. Structure relaxation

The static structure factor gives the correlation of local density at different spatial ranges at equilibrium. Insight into the timescale of the permanence of such correlations is provided by the intermediate scattering function, $F_{\alpha\beta}(\mathbf{k}, t)$, which measures structure relaxation at a given wavevector [37]:

$$F_{\alpha\beta}(\mathbf{k}, t) = \frac{1}{\sqrt{N_\alpha N_\beta}} \left\langle \sum_{i\in\alpha} \sum_{j\in\beta} \exp\{-\mathrm{i}\mathbf{k} \cdot [\mathbf{r}_i(t) - \mathbf{r}_j(0)]\} \right\rangle. \tag{2}$$

Several partial $F_{\alpha\beta}(\mathbf{k}, t)$ were calculated and examples are shown here in order to illustrate charge, concentration, and temperature effects on the timescale of the IRO dynamics. The calculated $S_{\alpha\beta}(k)$ shown in previous sections indicate that the interesting range to investigate cation–cation structural relaxation is $k \sim 0.8$ Å^{-1}. Figure 14 shows collective cation–cation $F_{\alpha\beta}(\mathbf{k}, t)$ for MCl, MCl_2, and MCl_3 solutions II, where we selected several vectors $\mathbf{k}$ in this range of modulus (0.7–0.9 Å^{-1}) in order to improve statistics. Increase of cation charge

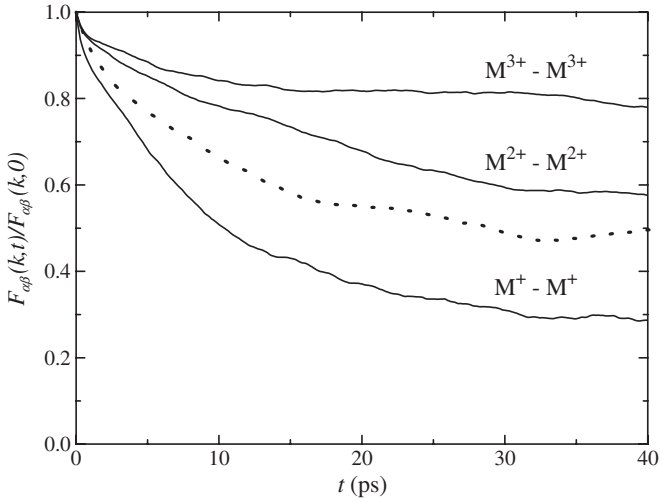

Figure 14. Partial cation–cation intermediate scattering functions, $F_{\alpha\beta}(\mathbf{k}, t)$, at $k = 0.8$ Å^{-1}, calculated by MD simulations of MCl, MCl_2, and MCl_3 solutions II. The corresponding result for MCl_3 solution II at 380 K is also shown by a dashed curve.

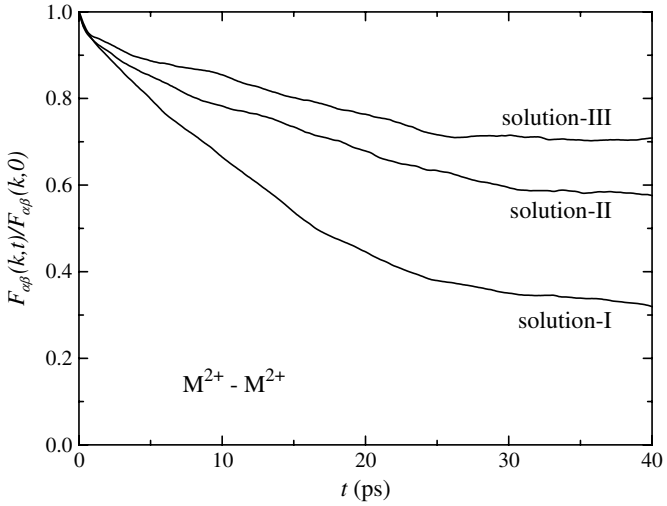

Figure 15. Partial cation–cation $F_{\alpha\beta}(\mathbf{k}, t)$ at $k = 0.8$ Å^{-1} calculated by MD simulations of MCl_2 solution I, solution II, and solution III.

dramatically slows down the IRO relaxation. It is clear that the lifetime of cation correlation in such a spatial range becomes very long in the case of high-valence cations. Figure 14 also shows, by a dotted curve, the corresponding result obtained by a physically reasonable increase in temperature (380 K) of the MCl_3 solution III. Thus, although the equilibrium structure is not very much affected by a slight increase in temperature (from 300 to 380 K), the corresponding IRO dynamics speeds up significantly. On the other hand, the concentration effect on the IRO relaxation is addressed in figure 15 for the three MCl_2 solutions. It is clear that by keeping the cation charge fixed and increasing the concentration, the IRO dynamics slows down significantly.

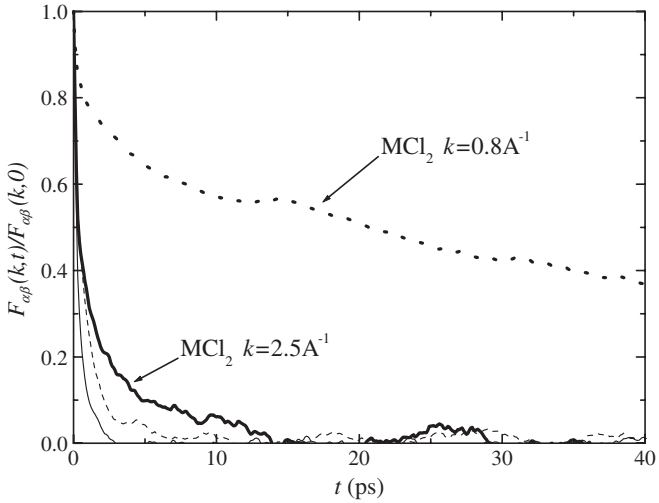

Figure 16. Partial water–water $F_{\alpha\beta}(\mathbf{k}, t)$ calculated by MD simulations of MCl_2 solution II at $k = 0.8$ Å^{-1} (dashed bold curve) and $k = 2.5$ Å^{-1} (full bold curve). For comparison purposes, corresponding results for pure water are shown by thin curves, $k = 0.8$ Å^{-1} (dashed thin curve) and $k = 2.5$ Å^{-1} (full thin curve).

One can appreciate how structural relaxation in ionic solutions is much slower than in pure water by investigating the partial water–water $F_{\alpha\beta}(\mathbf{k}, t)$. Figure 16 compares the water–water $F_{\alpha\beta}(\mathbf{k}, t)$ of the MCl_2 solution II and pure water at two different wavevectors, 0.8 and 2.5 Å^{-1}, that is, the pre-peak and the main peak of the corresponding $S_{\alpha\beta}(k)$, respectively (see figure 6). One sees that the $F_{\alpha\beta}(\mathbf{k}, t)$ decay more slowly in ionic solution than in pure water for both the k values, but the remarkable result is the dramatic slowing down of structural relaxation at $k \sim 0.8$ Å^{-1} in solution. In the case of pure water, $F_{\alpha\beta}(\mathbf{k}, t)$ at $k \sim 2.5$ Å^{-1} decays only slightly faster than $k \sim 0.8$ Å^{-1} because $k \sim 2.5$ Å^{-1} corresponds to the range of the broad main peak in $S_{\alpha\beta}(k)$. On the other hand, in the case of the MCl_2 solution II, the decaying of $F_{\alpha\beta}(\mathbf{k}, t)$ at $k \sim 0.8$ Å^{-1} is very slow. Therefore, the occurrence of IRO in aqueous ionic solution implies a corresponding IRO *dynamics* as structural relaxation in this spatial range is very much affected upon formation of the solution.

4. Conclusions

Computer simulations corroborate that IRO occurs in aqueous ionic solution when ions with elevated charge coexist with counter-ions of low charge. Systematic investigation by MD simulations of charge and concentration effects on the IRO supports the basic assumptions of the liquid-type quasi-close-packing model that has been successfully used in the interpretation of x-ray diffraction data of many ionic solutions [14–21]. Well defined correlation in position of high-charge cations is observed at relatively long distance, about 10.0 Å, which results, in reciprocal space, in a solid-like oscillatory pattern in the partial cation–cation $S_{\alpha\beta}(k)$. The first peak in this partial $S_{\alpha\beta}(k)$ is just in the range of observed pre-peaks in the experimental total $S(k)$ [14–21]. Partial water–water $S_{\alpha\beta}(k)$ also display a pre-peak in the case of M^{2+} or M^{3+} solutions due to water molecules that follow the cations in their hydration shell. Three other relevant findings are corroborated by MD simulations: the pre-peak shifts to higher wavevector with increasing concentration, the counter-ion will contribute destructively to the pre-peak if

its scattering power is made higher, and the pre-peak is washed out in case of a symmetric salt such as M^{2+} plus X^{2-}. A further detail that MD simulations provide that is not of concern in the quasi-close-packing model is the timescale of IRO relaxation. It has been found that correlation of density fluctuation in the spatial range of IRO, $k \sim 0.8$ Å^{-1}, would achieve hundreds of picoseconds until complete relaxation in the case of concentrated solutions of high-charge cations.

Acknowledgments

The author is indebted to FAPESP and CNPq for financial support.

References

[1] Peng Z, Ewig C S, Hwang M J, Waldman M and Hagler A T 1997 *J. Phys. Chem.* A **101** 7243
[2] Koneshan S, Rasaiah J C, Lynden-Bell R M and Lee S H 1998 *J. Phys. Chem.* B **102** 4193
[3] Spangberg D and Hermansson K 2004 *J. Chem. Phys.* **120** 4829
[4] Lyubartsev A P and Laaksonen A 1996 *J. Phys. Chem.* **100** 16410
[5] Chowdhuri S and Chandra A 2001 *J. Chem. Phys.* **115** 3732
[6] Zhu S B and Robinson G W 1992 *J. Chem. Phys.* **97** 4336
[7] Degreve L and da Silva F L B 1999 *J. Chem. Phys.* **111** 5150
[8] Zasetsky A Y and Svishchev I M 2001 *J. Chem. Phys.* **115** 1448
[9] Laudernet Y, Cartailler T, Turq P and Ferrario M 2003 *J. Phys. Chem.* B **107** 2354
[10] Botti A, Bruni F, Imberti S, Ricci M A and Soper A K 2004 *J. Chem. Phys.* **121** 7840
[11] Ebner C, Sansone R, Hengrasmee S and Probst M 1999 *Int. J. Quantum Chem.* **75** 805
[12] Heinje G, Luck W A P and Heinzinger K 1987 *J. Phys. Chem.* **91** 331
[13] Chang T M and Dang L X 2003 *J. Chem. Phys.* **118** 8813
[14] Marques M I B, Cabaço M I, Oliveira M A S and Marques M A 1982 *Chem. Phys. Lett.* **91** 222
[15] Marques M A and Cabaço M I 1986 *Chem. Phys. Lett.* **126** 551
[16] Cabaço M I, Marques M A, Marques M I B, Wye-Bushnell G, Costa M M and Almeida M J 1995 *J. Phys.: Condens. Matter* **7** 7409
[17] Cabaço M I, Gaspar A M, Morais C M and Marques M A 2000 *J. Phys.: Condens. Matter* **12** 2623
[18] Marques M A, Cabaço M I, Marques M I B, Gaspar A M and Morais C M 2001 *J. Phys.: Condens. Matter* **13** 4367
[19] Marques M A, Cabaço M I, Marques M I B and Gaspar A M 2002 *J. Phys.: Condens. Matter* **14** 7427
[20] Gaspar A M, Marques M A, Cabaço M I, Marques M I B, Buslaps T and Honkimaki V 2004 *J. Mol. Liq.* **110** 15
[21] Marques M A, Marques M I B, Cabaço M I, Gaspar A M and Almeida M L 2004 *J. Mol. Liq.* **110** 23
[22] Elliot S R 1990 *Physics of Amorphous Materials* (Harlow: Longman)
[23] Quitmann D and Soltwisch M 1998 *Phil. Mag.* B **77** 287
[24] Ribeiro M C C 2000 *Phys. Rev.* B **61** 3297
[25] Jin W, Kalia R K, Vashishta P and Rino J P 1994 *Phys. Rev.* B **50** 118
[26] Wilson M and Madden P A 1998 *Phys. Rev. Lett.* **80** 532
[27] Morineau D and Alba-Simionesco C 1998 *J. Chem. Phys.* **109** 8494
[28] Madden P A and Wilson M 2000 *J. Phys.: Condens. Matter* **12** A95
[29] Berendsen H J C, Grigera J R and Straatsma T P 1987 *J. Phys. Chem.* **91** 6269
[30] Chowdhuri S and Chandra A 2003 *J. Chem. Phys.* **118** 9719
[31] Tao N J, Li G, Chen X, Du W M and Cummins H Z 1991 *Phys. Rev.* A **44** 6665
[32] Feiweier T, Isfort O, Geil B, Fujara F and Weingartner H 1996 *J. Chem. Phys.* **105** 5737
[33] Ansell S, DupuyPhilon J, Jal J F and Neilson G W 1997 *J. Phys.: Condens. Matter* **9** 8835
[34] Suzuki Y and Mishima O 2002 *J. Chem. Phys.* **117** 1673
[35] Berendsen H J C, Postma J P M, Gunsteren W F, DiNola A and Haak J R 1984 *J. Chem. Phys.* **81** 3684
[36] Allen M P and Tildesley D 1987 *Computer Simulation of Liquids* (Oxford: Clarendon)
[37] Hansen J P and McDonald I R 1990 *Theory of Simple Liquids* (London: Academic)
[38] Barker D R, Wilson M, Madden P A, Medvedev N N and Geiger A 2000 *Phys. Rev.* E **62** 1427